Demonstration of an On-Chip TE-Mode Optical Circulator

Rui Ma, Sander F. G. Reniers, Yuya Shoji, *Member, IEEE*, Tetsuya Mizumoto, *Life Fellow, IEEE*, Yuqing Jiao, *Senior Member, IEEE*, Jos J. G. M. van der Tol, and Kevin A. Williams

Abstract— In this paper, an on-chip optical circulator on the InP-membrane-on-Si (IMOS) platform is demonstrated. The circulator is composed of two multi-mode interferometers (MMIs), four polarization converters (PCs), and a Cerium-doped Yttrium Iron Garnet (Ce:YIG) die. The Ce:YIG die is adhesively bonded on the InP membrane via a 125-nm thin bonding layer. Nonreciprocal phase shift (NRPS) is employed in the presence of a transverse magnetic field. The device works as a 4-port optical circulator with a maximum optical isolation of 27.0 dB and a minimum optical isolation of 18.6 dB for the TE mode. The measured optical isolation bandwidth is 0.12 nm. Two methods are proposed in order to improve the optical isolation bandwidth.

Index Terms— Magnetooptic devices, optical circulators, integrated optics, polarization.

I. INTRODUCTION

THE InP-membrane-on-Si (IMOS) platform is promising for the integration of nano-photonics with high performance active devices [1]. In the IMOS platform, various of active and passive devices, like lasers, photodiodes, modulators, and polarization converters (PCs), are demonstrated [2]. For the next level up with single chip implementations for fibre sensor interrogators, optical imaging systems and PON transceivers, optical circulators are needed in the IMOS platform.

Optical circulators are extensions of isolators, as they separate signals travelling in opposite directions, e.g., supporting bi-directional transmission. The key to achieve optical isolation is to break the Lorentz reciprocity. However, due to the reciprocal nature of most semiconductor and dielectric materials, the integration of optical nonreciprocal devices with other integrated optical components presents crucial design and fabrication challenges [3].

In recent years, on-chip optical nonreciprocal devices, based on heterogeneous integration of Ce:YIG on the semiconductor

platform have been investigated [4]. Mainly three approaches are developed: i) Pulsed laser deposition (PLD) [5], ii) Direct bonding [6] and iii) Adhesive bonding [7].

Among them, the last approach is the most suitable for the IMOS platform. The Ce:YIG layer needs over 800 °C annealing temperature to crystalize [8], which is beyond the epitaxial growth temperature of III/V semiconductor. Direct bonding on the other hand is not suitable for the IMOS platform, due to the presence of surface topology.

The IMOS platform is aiming at achieving complex and high-density PICs, where back reflections with unknown polarization states may occur. Hence, polarization-independent circulators are needed in the circuits. However, for circulators bonded with Ce:YIG films, although both TE and TM modes interact with Ce:YIG, and they both experience absorption loss, only the TM mode experiences a nonreciprocal phase shift (NRPS), in the presence of an external magnetic field [9]. Since the output light from most lasers or SOAs is TE polarized [10], it is more important to develop optical circulators for TE mode rather than TM mode.

In order to achieve integrated optical TE-mode circulators, a widely developed solution is to implement TE-TM polarization converters (PCs) with TM-mode circulators. In 2019, a TE-mode circulator, with an isolation ratio as large as 30 dB, was demonstrated [11]. In this design, PCs are placed at all the MZI-ports to enable optical circulation for the TE mode input. However, these PCs are based on mode hybridization [12] and requires strict critical dimension control in the fabrication process. In 2021, an integrated optical circulator, with maximum optical isolations of 27.0 dB for TE mode input and 34.0 dB for TM mode input, was demonstrated [13]. By implementing two PCs in one arm of a MZI based TM-mode circulator, this device can be operated for the two modes. However, further improvements, such as reducing the phase error between the two arms, increasing the isolation bandwidth, are still needed in order to claim a truly polarization-independent circulator for practical applications.

In this paper, an on-chip TE-mode circulator is proposed on the IMOS platform, which is promising for the next-generation PIC with compact footprint and low power consumption. Ultra-small (<5 μm length) and efficient ($>97.5\%$ polarization conversion efficiency) PCs are implemented to achieve TE mode operation [14]. In order to obtain sufficiently large NRPS for the TM mode, while maintaining a relatively large bonding tolerance. Optimized bonding layer thickness and size of Ce:YIG are obtained by simulations. An multi-die-to-wafer

Fig. 1. Schematic of the on-chip optical circulator.

Fig. 2. (a) Side view of a PC. (b) Coordinate transformation to new bases.

bonding procedure is developed to integrate the Ce:YIG dies with the InP membrane. The device is characterized as a 4-port circulator. Solution to increase the optical isolation bandwidth of the device are also proposed.

II. DEVICE DESIGN

The schematic of the on-chip optical circulator is shown in Fig. 1. The device is based on a Mach-Zehnder interferometer (MZI). Two 2×2 multimode interferometers (MMIs) are placed on both sides of the device to form a 4-port circulator.

Four PCs are involved in the two arms. Fig. 2(a) is a scanning electron microscope (SEM) image of the PC in the IMOS platform. It contains two triangular waveguides with one rectangular waveguide section in between. A new set of eigenmodes are excited in the triangular section when a TE or TM mode from the straight waveguide is coupled to it.

As shown in Fig. 2(b), the new set of eigenmodes M1 and M2 is not aligned with the TE/TM polarizations of normal rectangular waveguides. As the eigenmodes propagate at different phase velocities, a phase-shift $\Delta\varphi$ will be created after the propagation length l.

$$\Delta\varphi = |\beta_1 - \beta_2| \cdot l \tag{1}$$

where β_1 and β_2 are the propagation constants of two eigenmodes M1 and M2. After propagating over a certain length in the triangular sections, the two modes will recombine to different elliptical and linear polarization states in the rectangular waveguide section. By optimizing the lengths of the two triangular waveguide sections, a full TE-TM conversion can be achieved.

A Ce:YIG die is adhesively bonded on top of two arms of the MZI structure with a layer of benzocyclobutene (BCB). The NRPS effect will be present for the TM mode when an external lateral magnetic field is applied. TE and TM modes have different propagation constants in the rectangular waveguide sections, which will introduce a reciprocal phase shift (RPS) to the propagating light in the two arms.

In the forward direction, the input signal coupled into port 1 is split into two arms by a 2×2 MMI. When the input is the TE mode, it will be converted to the TM mode after passing through PC 1 in the upper arm. NRPS becomes effective on the TM mode when a transverse magnetic field is applied. A NRPS of $\pi/2$ can be achieved by optimizing the interaction of the light with the Ce:YIG layer. The TM mode will be converted back to TE mode after PC 2.

In the lower arm, the TE mode will not be affected by the NRPS effect. The TE mode signal in the lower arm will be converted to TM mode after PC 3 and be converted back to TE
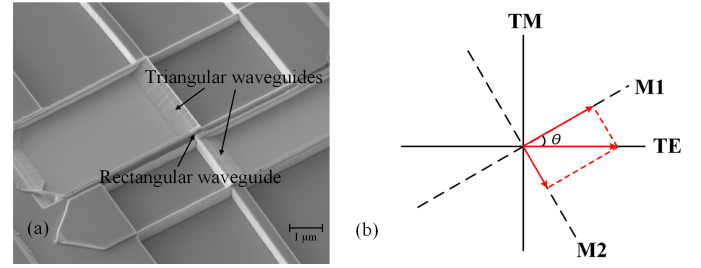
mode after PC 4. PC 3 and PC 4 are used to balance the optical powers in the two arms before they enter the second 2×2 MMI. The birefringence in the two arms causes a reciprocal $\pi/2$ phase shift. When both signals are combined in the output MMI, a total phase difference of π is presented. Thus, the output signal will emerge from port 2. Similarly, inputs from port 3 will appear from port 4.

For the backward direction, the NRPS has the opposite sign. Therefore, the TE input signal launched in port 2(4) will emerge in port 3(1) by cancelling the phase difference between the two arms. Hence, the device works as a 4-port optical circulator for the TE mode.

III. OPTIMIZATION OF THE DESIGN PARAMETERS

In order to achieve a sufficiently large NRPS, the design parameters, such as the thickness of the bonding layer and the length of the Ce:YIG layer, need to be optimized to enable a strong evanescent coupling, while reducing optical absorption loss from the Ce:YIG layer. In the meanwhile, the presence of the bonded layer brings extra loss and reflection, due to mode mismatch at the interface. Thus, it is important to find a trade-off between these device performances and the footprint in simulations.

The typical InP waveguide in the IMOS platform is 400 nm in width and 300 nm in height. A 500 nm thick Ce:YIG film (refractive index: 2.2) is sputtered on a SGGG substrate (refractive index: 1.9) and has a Faraday rotation coefficient of 4500 °/cm at 1550 nm.

To model the NRPS effect, two permittivity tensors for forward and backward propagation directions are written as (the magnetic field is in the y direction in Fig. 1):

$$\varepsilon_{forward} = \begin{pmatrix} 2.2^2 & 0 & \varepsilon_{xz} \\ 0 & 2.2^2 & 0 \\ -\varepsilon_{xz} & 0 & 2.2^2 \end{pmatrix} \tag{2}$$

$$\varepsilon_{backward} = \begin{pmatrix} 2.2^2 & 0 & -\varepsilon_{xz} \\ 0 & 2.2^2 & 0 \\ \varepsilon_{xz} & 0 & 2.2^2 \end{pmatrix} \tag{3}$$

where $\varepsilon_{xz} = ig_y$. g_y is the gyration vector of the Ce:YIG layer in the y direction, which is transverse to the propagation direction of the light [15]. g_y is 0.009 when the Ce:YIG layer is saturated by the y-direction magnetic field. This value corresponds to the 4500 °/cm Faraday rotation coefficient of Ce:YIG.

The TM mode light will experience different propagation constant in the forward and backward directions. The NRPS
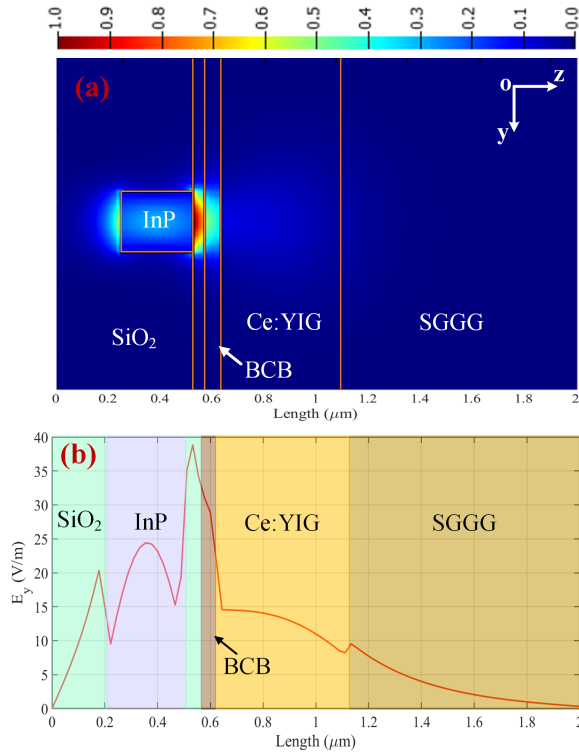
Fig. 3. (a) Electrical field profile of the TM mode. (b) Electric field distribution of the TM mode in the vertical direction.

can be expressed as:

$$NRPS = (\beta_{forward} - \beta_{backward}) \cdot L_2 \qquad (4)$$

where $\beta_{forward}$ and $\beta_{backward}$ are the propagation constants of the TM mode light in forward and backward propagation, respectively. L_2 is the length of the waveguide coated with Ce:YIG.

NRPS as a function of the thickness of the bonding layer is analyzed using a finite-difference time-domain (FDTD) solver. The simulated NRPS is decreasing with increased BCB thickness. It is found that a 122 nm thick bonding layer (a 50 nm SiO$_2$ layer and a 72 nm BCB layer) is needed to reach π rad NRPS for a Ce:YIG layer with 4 mm length.

The electric field profile of the TM mode is shown in Fig. 3(a). A 50 nm SiO$_2$ layer is deposited on the waveguide to enhance the adhesion of BCB. Then, the InP waveguide is covered with a 72 nm thick BCB layer. A Ce:YIG layer on a SGGG substrate is bonded on top of the BCB and serves as a top-cladding layer.

The electric field distribution in the z direction of the TM mode is shown in Fig. 3(b), it can be seen that a large portion of the electrical field is confined in the bonding layer. For the TM mode, the confinement factor in the Ce:YIG layer is 17.4% if the thickness of the bonding layer is 122 nm. The calculated confinement factor of the TE mode is 5.3%. Considering that the optical absorption loss of the Ce:YIG at 1550 nm is 42 dB /cm [16], the calculated absorption losses are 0.9 dB and 2.8 dB for the two modes.

Owing to the mode mismatch between the waveguide with air cladding and the waveguide with Ce:YIG cladding, loss and reflection are induced at the interfaces. This is affected
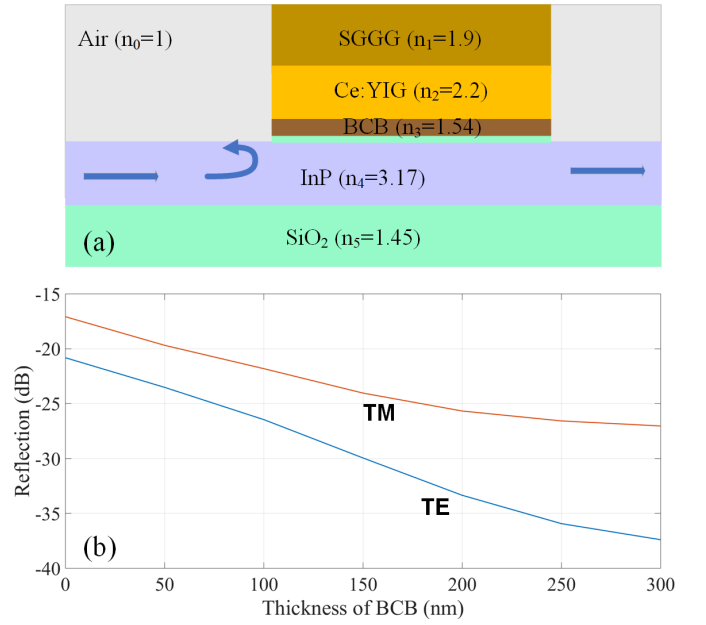

Fig. 4. (a) Side view of the InP waveguide bonded with Ce:YIG. (b) Reflection at the interface as a function of the BCB thickness.

by the thickness of the bonding layer, as indicated in Fig. 4(a). In Fig. 4(b), reflection at the interface as a function of the BCB thickness for the TE and TM mode at a wavelength of 1550 nm are shown, as simulated with a FDTD solver.

It can be seen that the reflection is decreasing with increasing BCB thickness for both TE and TM mode. The TM mode in the cladding undergoes more reflection than the TE mode because of its larger confinement factor. In these simulations, it is assumed that the Ce:YIG layer has no optical absorption. When the thickness of BCB is 72 nm, the loss due to the edges of the Ce:YIG cladding for the two polarization states is below 1 dB and the reflection is below 20 dB.

In summary, for a 4 mm long Ce:YIG die, a 50 nm thick SiO$_2$ and a 72 nm thick BCB layer for the bonding layer are found to give sufficient NRPS, while shortening the device dimension, reducing the insertion loss and maintaining the fabrication tolerance.

IV. FABRICATION PROCESS

The Ce:YIG-die-to-IMOS-wafer bonding process is illustrated in Fig. 5.

First, a surface cleaning process is performed. The IMOS wafer is rinsed in acetone, Isopropylalchohol (IPA) and ultra-pure water (UPW) consecutively to remove dirt on the surface. Immediately afterwards, an oxygen plasma stripping process is performed to remove organic residuals on the surface. Subsequently, a diluted H$_3$PO$_4$ rinsing step is used to remove semiconductor oxides after oxygen stripping.

A 50 nm SiO$_2$ layer is deposited on the wafer as an adhesion layer for BCB. Then, the wafer is baked at 280 °C in a vacuum oven in order to evaporate any water vapor and to remove remaining gaseous inclusions in SiO$_2$.

Before BCB spin-coating, a layer of adhesion promoter AP3000 is spin-coated and soft-baked at 135 °C for 5 minutes, to improve the adhesion of BCB on SiO$_2$. The spin coating of
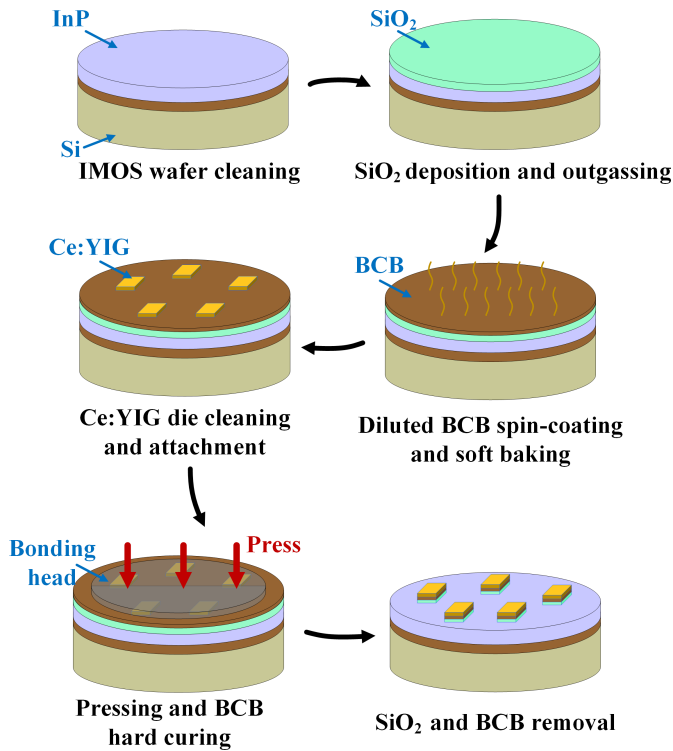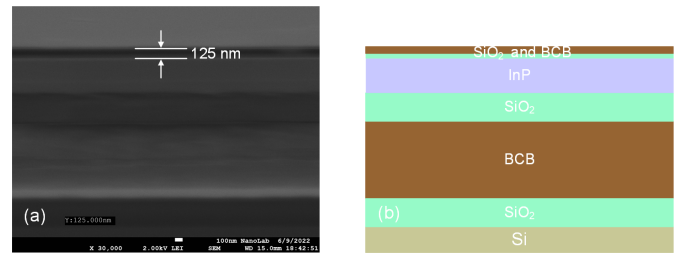
Fig. 5. The Ce:YIG-die-to-IMOS bonding process.

Fig. 6. (a) SEM image of the cross-section of the IMOS wafer with a thin bonding layer on the surface. (b) Identification of different layers in (a).
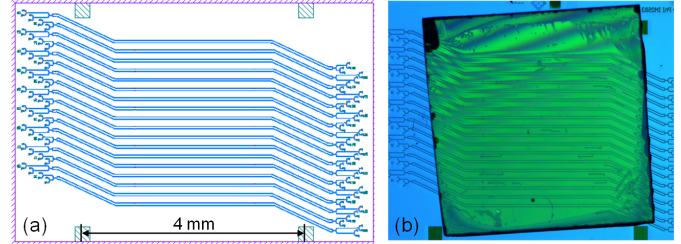

Fig. 7. (a) The designed mask. (b) Microscope image of the fabricated devices bonded with a Ce:YIG die.

AP3000 results in a layer of silanol group molecules, which react with free hydroxyl groups on an oxidized silicon wafer surface. In this way, the adhesion of the BCB is improved. Compared with the thickness of the bonding layer (over 100 nm), this monolayer of molecules does not affect the light confinement. Thus, it is neglected in optical simulations. Then, a layer of diluted BCB is spin-coated on the SiO_2 layer. Next, the wafer is soft-baked to evaporate the remaining solvent from the BCB. The temperature for soft-baking is 135 °C, with a ramp of about 5 °C /min.

Multiple Ce:YIG dies (4 mm × 4 mm) are cleaned using acetone and IPA. They are aligned and attached manually on the IMOS wafer. The Ce:YIG dies and the IMOS wafer are loaded in the bonder. The bonding process starts with evacuating the chamber to 1×10^{-3} mbar and increasing the temperature to 50 °C with a ramp of 5 °C /min. Immediately afterwards, the Ce:YIG dies and the IMOS wafer are brought into contact for 10 minutes, by applying 170 N force with a piston, at a temperature of 140 °C. The BCB layer is still in a liquid phase at this temperature, so it can fill in the voids at the bonding interface. Then, the pressure of the chamber increases to 800 mbar with a N_2 atmosphere. The dies and the wafer reach to 280 °C with a ramp of 5 °C/min. The full cross-linking of the BCB layer is achieved at this temperature. Finally, the chamber is cooled to 50 °C and the sample is ready to be unloaded.

In the IMOS platform, the center wavelength of the grating couplers, used for coupling light into and out of the chip, is optimized at 1550 nm with an air cladding. The presence of the bonding layers on the grating couplers will cause an unwanted wavelength shift. Therefore, after the bonding

process is finished, a RIE process is performed to etch away the SiO_2 and BCB layer outside of the bonding area.

To measure the BCB thickness, an IMOS wafer bonded with Ce:YIG dies is cleaved. A SEM image of the cross-section of the bonded wafer is shown in Fig. 6(a).

The Ce:YIG die is not present in the image since it came off during the cleaving process. The measured thickness of the bonding layers (a SiO2 layer and a BCB layer) is around 125 nm. This measurement result matches well with the target value. According to the simulation results, this BCB thickness is close to the values needed for reaching π rad NRPS, when the length of the Ce:YIG die is 4 mm.

The designed mask pattern is shown in Fig. 7(a). The four squares are designed to align the four corners of the Ce:YIG die. The length of the rectangular waveguide in between the two PCs is 5.8 mm, to ensure enough space for the Ce:YIG die placement during the Ce:YIG-die-to-IMOS-wafer bonding process.

Fig. 7.(b) is a microscope image of the fabricated wafer. It can be seen that a 4×4 mm^2 Ce:YIG die is adhesively bonded to the InP waveguide. When the Ce:YIG film is saturated, the NRPS is expected to be π rad for different propagation directions according to the simulation results. The corners of the die deviate from the squares. This is because the die is manually aligned, and it might move during wafer handling and transferring. This misalignment does not affect the measurement since all the grating couplers are outside of the bonding area.

V. CHARACTERIZATION

A schematic of the measurement setup is given in Fig. 8. The grating couplers are designed to couple light into or out of the device to the fibers. The two single mode fibers are aligned to the gratings at an angle of 10° with respect to the surface normal. TE light can be injected and collected using the grating couplers. A Nd-Fe-B magnet is attached on top of the SGGG substrate to create a transverse magnetic field
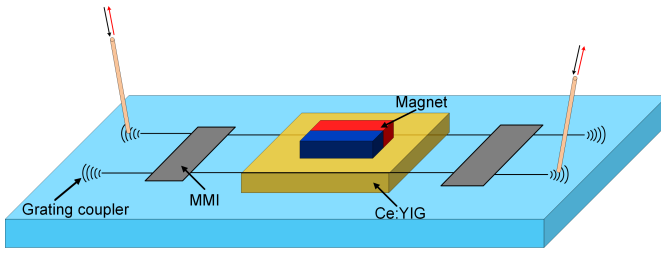
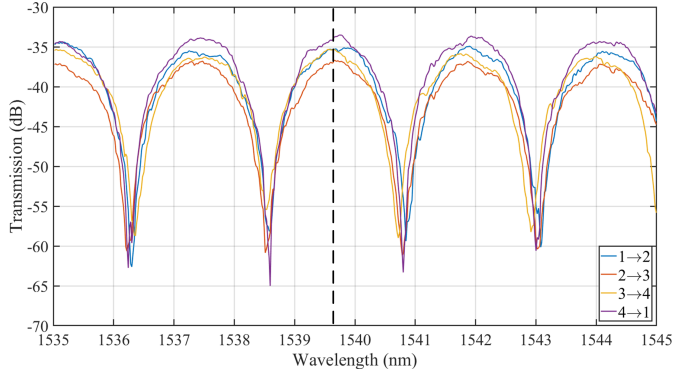Fig. 8.   Schematic of the characterization setup.

Fig. 9.   Transmission spectra between different ports for TE mode input in clockwise direction.
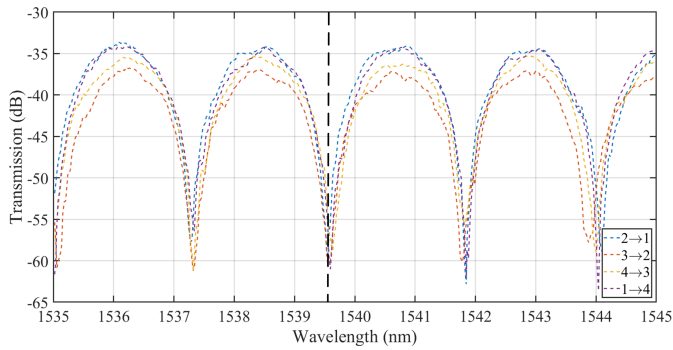

Fig. 10.   Transmission spectra between different ports for TE mode input in counterclockwise direction.

in the Ce:YIG film. The magnetic field at the Ce:YIG film is strong enough to saturate the Ce:YIG film (over 50 Oe).

The transmission spectra are recorded from the grating couplers for the forward and backward propagation direction in order to characterize the nonreciprocity of the device.

The measured transmission between port pairs on opposite sides of the circulator are presented in Fig. 9 and Fig. 10, for two opposite directions respectively. Over 20 dB extinction ratio of the MZI for different port pairs are obtained. This indicates a fairly well-balanced power in the two arms. The power difference in the two arms is affected by various factors, such as the polarization-dependent (PD) optical absorption in Ce:YIG, the PD propagation loss, the PD reflection at the interface between plain InP waveguide and garnet-covered waveguide. As discussed in the second section, the Ce:YIG has higher absorption for TM mode than TE mode. In the meanwhile, the TE mode suffers from more propagation loss from the sidewall roughness, due to the mode distribution in the waveguide. All these factors contribute to the losses in the two arms and result in a large extinction ratio. However,

TABLE I
INSERTION LOSS ANALYSIS

Sources of loss	Value (dB)
Fiber-to-waveguide coupling loss	13.8 (measured)
Loss in two 2×2 MMIs	2.0 (estimated)
Loss in four PCs	4.0 (estimated)
Propagation loss in the waveguide	11.0 (measured)
Coupling loss in the 1×2 MMI	3.0 (estimated)
Ce:YIG-bonding-induced loss	3.0 (measured)
Total	36.8

further characterizations are needed to investigate the exact contributions of these factors.

The nonreciprocal circulator functionality is clearly visible by comparing Fig. 9 and Fig. 10. The transmittance for the clockwise direction at a wavelength of 1539.6 nm is between −36.9 dB and −34.0 dB, and for counterclockwise direction between −61.0 dB and −54.5 dB. The isolation ratio computed between two opposite ports reaches a maximum value of 27.0 dB, while a minimum isolation of 18.6 dB is found. For the PCs implemented in this device, the measured polarization conversion efficiency (PCE) is 96%±0.5%, using a 4-port characterization method [14]. This incomplete conversion contributes to the transmittance differences among the port pairs.

The various sources of excess loss of the device are analyzed in Table I. The fiber-to-waveguide coupling loss is measured as 13.8 dB. A 1×2 MMI is placed at the output port to split the light to two grating couplers. The PC gives around 1.0 dB loss and the 2 × 2 MMI gives around 1.0 dB loss. Another 3.0 dB loss is observed from the device with Ce:YIG compared to the device without Ce:YIG. This excess loss is attributed to optical absorption of Ce:YIG, and to scattering and reflection at the boundaries between BCB and Ce:YIG cladding regions. The remaining insertion loss is attributed to the propagation loss of the waveguide, which is around 11.0 dB. This large waveguide loss is attributed to the sidewall roughness induced during the EBL step. This can be optimized by utilizing 193-nm Deep UV Lithography, which could reduce the waveguide loss significantly [17]. The insertion losses can be further improved by shortening the length of the Ce:YIG die (the length of the waveguide section covered with Ce:YIG is shortened as well then), and by optimizing the design of the PCs and MMIs.

In Fig. 4(b), −25 dB reflection is obtained when the BCB thickness is about 70 nm. To characterize possible back reflections, input and output fibers are placed at port 1 and port 3, respectively. The measured reflection gets close to the noise floor of the photodetector (around −60 dBm). This is because of the existence of the high excesses losses as shown in Table I. Further investigation is needed to quantify the back-reflection.

It can also be obtained that the FSR of this device is about 2.3 nm. The optical isolation bandwidth represents a wavelength range in which the optical isolation is at most 3 dB less than the maximum optical isolation value. The measured optical isolation bandwidth for the two polarization states is 0.12 nm. In the design, the two arms of the MZI have the same

length. However, there is always a TE mode in one arm and a TM mode in the other arm, regardless of whether the input is the TE or TM mode. The different propagation constants of the two modes result in an imbalance of the MZI. For practical application purposes, a larger bandwidth is needed.

In the forward direction, the phase shift in the upper arm and the lower arm can be expressed as following if a TE mode light is injected:

$$\varphi_{up} = \beta_{TM,1} \cdot L_1 + \beta_{TM,2} \cdot L_2 + \beta_{TE,1} \cdot L_3 \tag{5}$$

$$\varphi_{bot} = \beta_{TE,1} \cdot L_1 + \beta_{TE,2} \cdot L_2 + \beta_{TM,1} \cdot L_3 \tag{6}$$

where L_1 is the length of the waveguide without coated Ce:YIG between two PCs in the upper arm, and $\beta_{TE,1}$ and $\beta_{TM,1}$ are the corresponded propagation constants of the two modes. L_2 is the length of the waveguide with coated Ce:YIG between two PCs in the upper arm, and $\beta_{TE,2}$ and $\beta_{TM,2}$ are the corresponded propagation constants of the two modes.

The expected phase difference between two arms can be expressed as:

$$\Delta\varphi = (\beta_{TM,1} - \beta_{TE,1}) \cdot (L_1 - L_3) + (\beta_{TM,2} - \beta_{TE,2}) \cdot L_2 \tag{7}$$

The effective refractive indices of the two modes in the waveguides with and without Ce:YIG are obtained from a mode solver:

$$\Delta n_{eff,1} = \left| n_{TE,1} - n_{TM,1} \right| = 0.22 \tag{8}$$

$$\Delta n_{eff,2} = \left| n_{TE,2} - n_{TM,2} \right| = 0.16 \tag{9}$$

Hence, the phase difference $\Delta\varphi$ can be expressed as:

$$\Delta\varphi = (\beta_{TM,1} - \beta_{TE,1}) \cdot (L_1 + 0.73L_2 - L_3) \tag{10}$$

Light in the two arms becomes in-phase at the output if $\Delta\varphi = 2n\pi$ (n is an integer). In order to increase the optical isolation bandwidth, the integer n should be as small as possible. Therefore, the bandwidth can be improved by either reducing L_1 and L_2 or increasing L_3.

In this design, L_1 is 1.8 mm, L_2 is 4 mm and L_3 is 20 μm. This results in a large imbalance of the MZI, and hence a narrow isolation bandwidth. In order to increase the bandwidth, while maintaining large optical isolation, two methods can be used:

(1) Using shorter Ce:YIG dies and thinner bonding layers. For example, for a device with a 2 mm long Ce:YIG die and a 68 nm thick bonding layer, the predicted optical isolation is over 30 dB, and the predicted bandwidth is about 0.3 nm. To achieve a thinner bonding layer, the SiO$_2$ and BCB thicknesses should be reduced. In this paper, the SiO$_2$ thickness is 50 nm deposited by a plasma-enhanced chemical vapor deposition (PECVD) tool. This thickness can be reduced by reducing the deposition time in PECVD or using an Atomic layer deposition (ALD) tool. The BCB thickness is mainly determined by the BCB to solvent(mesitylene) dilution ratio. A thinner BCB layer can be obtained if the dilution ratio is decreased.

(2) Implementing two optical delay lines in the two arms. In this way, the bandwidth can be increased to tens of nanometers since L_3 could be close to $(L_1 + 0.73L_2)$.

Therefore, this device is promising for practical applications with improved bandwidth.

VI. CONCLUSION

In this work, a 4-port on-chip optical circulator for TE mode light is demonstrated, realized with an adhesively bonded Ce:YIG die to a MZI-based structure, fabricated on the IMOS platform.

A multiple-Ce:YIG-die-to-InP-membrane adhesive bonding procedure is developed. An ultra-thin BCB bonding layer is achieved to adhesively bond multiple Ce:YIG dies to the InP membrane. The measured thickness of the bonding layer is 125 nm, which is sufficient for evanescent coupling between the 4 mm long Ce:YIG die and a InP waveguide. This heterogeneous integration technique also offers the potential of bonding other functional materials on the InP membrane platform.

This device shows a maximum optical isolation of 27.0 dB and a minimum optical isolation of 18.6 dB for TE mode light. Sources of the insertion losses are also studied. The measured optical isolation bandwidth is 0.12 nm, The reason of this narrow bandwidth is found, and two methods to increase the bandwidth are proposed. The device can be integrated with other photonic components, like lasers and amplifiers.

ACKNOWLEDGMENT

REFERENCES

[1] J. J. G. M. van der Tol, Y. Jiao, J. P. Van Engelen, V. Pogoretskiy, A. A. Kashi, and K. Williams, "InP membrane on silicon (IMOS) photonics," *IEEE J. Quantum Electron.*, vol. 56, no. 1, pp. 1–7, Feb. 2020.

[2] Y. Jiao et al., "InP membrane integrated photonics research," *Semicond. Sci. Technol.*, vol. 36, no. 1, pp. 1–26, 2020.

[3] D. Huang, P. Pintus, and J. E. Bowers, "Towards heterogeneous integration of optical isolators and circulators with lasers on silicon [invited]," *Opt. Mater. Exp.*, vol. 8, no. 9, p. 2471, Sep. 2018.

[4] W. Yan, Y. Yang, W. Yang, J. Qin, L. Deng, and L. Bi, "On-chip nonreciprocal photonic devices based on hybrid integration of magneto-optical garnet thin films on silicon," *IEEE J. Sel. Topics Quantum Electron.*, vol. 28, no. 3, pp. 1–15, May 2022.

[5] Y. Zhang et al., "Monolithic integration of broadband optical isolators for polarization-diverse silicon photonics," *Optica*, vol. 6, no. 4, p. 473, Apr. 2019.

[6] Y. Shoji and T. Mizumoto, "Magneto-optical non-reciprocal devices in silicon photonics," *Sci. Technol. Adv. Mater.*, vol. 15, no. 1, Feb. 2014, Art. no. 014602.

[7] S. Ghosh, S. Keyvavinia, W. Van Roy, T. Mizumoto, G. Roelkens, and R. Baets, "Ce:YIG/silicon-on-insulator waveguide optical isolator realized by adhesive bonding," *Opt. Exp.*, vol. 20, no. 2, p. 1839, Jan. 2012.

[8] L. Bi et al., "Magneto-optical thin films for on-chip monolithic integration of non-reciprocal photonic devices," *Materials*, vol. 6, no. 11, pp. 5094–5117, Nov. 2013.

[9] S. Ghosh, S. Keyvavinia, W. Van Roy, T. Mizumoto, G. Roelkens, and R. Baets, "Ce:YIG/silicon-on-insulator waveguide optical isolator realized by adhesive bonding," *Opt. Exp.*, vol. 20, no. 2, p. 1839, Jan. 2012.

[10] A. R. Adams, "Strained-layer quantum-well lasers," *IEEE J. Sel. Topics Quantum Electron.*, vol. 17, no. 5, pp. 1364–1373, Sep. 2011.

[11] P. Pintus, D. Huang, P. A. Morton, Y. Shoji, T. Mizumoto, and J. E. Bowers, "Broadband TE optical isolators and circulators in silicon photonics through Ce: YIG bonding," *J. Lightw. Technol.*, vol. 37, no. 5, pp. 1463–1473, Mar. 1, 2019.

[12] D. Dai and J. E. Bowers, "Novel concept for ultracompact polarization splitter-rotator based on silicon nanowires," *Opt. Exp.*, vol. 19, no. 11, pp. 10940–10949, 2011.

[13] R. Ma et al., "Integrated polarization-independent optical isolators and circulators on an InP membrane on silicon platform," *Optica*, vol. 8, no. 12, pp. 1654–1661, 2021.

[14] S. F. G. Reniers, K. A. Williams, J. J. G. M. van der Tol, and Y. Jiao, "An accurate characterization method for integrated polarization converters," *IEEE J. Quantum Electron.*, vol. 57, no. 1, pp. 1–6, Feb. 2021.

[15] H. Zhou, J. Chee, J. Song, and G. Lo, "Analytical calculation of non-reciprocal phase shifts and comparison analysis of enhanced magneto-optical waveguides on SOI platform," *Opt. Exp.*, vol. 20, no. 8, p. 8256, Apr. 2012.

[16] Y. Shoji, M. Ito, Y. Shirato, and T. Mizumoto, "MZI optical isolator with Si-wire waveguides by surface-activated direct bonding," *Opt. Exp.*, vol. 20, no. 16, pp. 18440–18448, 2012.

[17] J. Van Engelen, S. Reniers, J. Bolk, K. Williams, J. J. G. M. Van Der Tol, and Y. Jiao, "Low loss InP membrane photonic integrated circuits enabled by 193-nm deep UV lithography," *CSW Proc.*, vol. 35, pp. 35–36, May 2019.

Rui Ma received the B.Eng. degree from the Beijing Institute of Technology, Beijing, China, in 2015, and the M.Sc. (Eng.) degree from the Institute of Semiconductors, Chinese Academy of Sciences, in 2018. He is currently pursuing the Ph.D. degree with the Photonic Integration (PhI) Group, Eindhoven University of Technology, in 2018. His research interests include integrated optical nonreciprocal devices, heterogeneous integration technology, and development of the IMOS platform.

Sander F. G. Reniers was born in Hapert, The Netherlands, in 1986. He received the B.Sc. degree in electrical engineering and the M.Sc. (cum laude) and Ph.D. degrees from the Eindhoven University of Technology, The Netherlands, in 2014, 2017, and 2022, respectively. During his bachelor's final project, he got in touch with photonic integration for the first time with the Eindhoven University of Technology. During his M.Sc. studies, he spent nine months at Oclaro (now Lumentum), Caswell, U.K., for his thesis work. The topic of his thesis is integration and characterization of advanced functionality on the IMOS platform, focusing on bringing polarization handling to the platform. He is currently working as a Post-Doctoral Researcher in micro-transfer-printing of indium phosphide coupons.

Yuya Shoji (Member, IEEE) received the B.E., M.E., and Ph.D. degrees in electrical engineering from the Tokyo Institute of Technology, Tokyo, Japan, in 2003, 2005, and 2008, respectively. He was a Post-Doctoral Fellow with the National Institute of Advanced Industrial Science and Technology, Tsukuba, Japan, from 2008 to 2010. He was an Assistant Professor with the Graduate School of Science and Engineering, Tokyo Institute of Technology, from 2011 to 2014, where he is currently an Associate Professor with the Laboratory for Future Interdisciplinary Research of Science and Technology (FIRST). His current research interests include device designs and fabrication of magneto-optical devices, silicon nanophotonic devices, and the photonic integrated circuits.

He is also a member of Optical Society of America, The Institute of Electronics, Information and Communication Engineers, the Japan Society of Applied Physics, and the Magnetic Society of Japan.

Tetsuya Mizumoto (Life Fellow, IEEE) received the B.E degree in electrical and electronic engineering, the M.E. degree in physical electronics, and the D.Eng. degree in electrical and electronic engineering from the Tokyo Institute of Technology (Tokyo Tech), Tokyo, Japan, in 1979, 1981, and 1984, respectively.

He worked with Tokyo Tech in April 1984 as a Research Associate at the Faculty of Engineering and became an Associate Professor in March 1987. He was promoted to a Full Professor with the Graduate School of Engineering in April 2004. From October 2012 to March 2018, he worked as the Vice President for Education with Tokyo Tech and became the Executive Vice President for Education in April 2018. His research interests include applied optics, photonic circuits, information and communication engineering, and waveguide optical devices, especially magneto-optic devices and all-optical switching devices based on the third-order nonlinearity.

Dr. Mizumoto is a fellow of Information and Communication Engineers (IEICE) and a member of the Japan Society of Applied Physics and the Magnetic Society of Japan. He was a recipient of the Treatise Award in 1994 and the Best Letter Award of Electronics Society Transactions in 2007 from the Institute of Electronics and IEICE. He was also a recipient of the Institute of Electrical and Electronics Engineers (IEEE) Photonics Society Distinguished Lecturer Awards in July 2009, IEEE Fellow Grade for "Contributions to investigations of waveguide optical nonreciprocal devices for optical communications" in January 2012, and the IEICE Achievement Award for "Pioneering work on optical nonreciprocal circuits" in May 2012.

Yuqing Jiao (Senior Member, IEEE) was born in Hangzhou, China. He received the dual Ph.D. degrees from the Eindhoven University of Technology, The Netherlands, and Zhejiang University, China, in 2013. Since 2013, he has been involved in the research at the Eindhoven University of Technology, where he has been an Assistant Professor with the Institute of Photonic Integration (IPI, former COBRA Research Institute) since 2016. He is focusing on ultrafast and strong light-matter interactions in sub-micron optical confinement. His applications span from optical interconnects, ultrafast photonic devices, to optical beam steering, and optical sensing. He has strong background and expertise in a wide range of photonic materials (from silicon to III–V) and nanotechnologies. He has coauthored more than 30 international journal publications and 70 conference articles. His research interests include novel III–V-based nanophotonic platform. He is a member of the IEEE Photonics Society and the Optical Society of America. He currently serves as a Board Member for the IEEE Photonics Society Benelux Chapter.

Jos J. G. M. van der Tol received the M.Sc. and Ph.D. degrees in physics from the State University of Leiden, The Netherlands, in 1979 and 1985, respectively. In 1985, he joined KPN Research, where he became involved in research on integrated optical components for use in telecommunication networks. Since July 1999, he has been an Associate Professor with the Eindhoven University of Technology, The Netherlands, where his research interests include opto-electronic integration, polarization issues, photonic membranes, and photonic crystals. Furthermore, he has been working on guided wave components on III–V semiconductor materials. He has also been active in the field of optical networks, focusing on survivability, introduction scenarios, and management issues. He has coauthored more than 250 publications in the fields of integrated optics and optical networks. He has 25 patent applications to his name. His research interests include the modeling of waveguides and design of electro-optical devices on lithium niobate and their fabrication.

Kevin A. Williams received the B.Eng. degree from the University of Sheffield, Sheffield, U.K., and the Ph.D. degree from the University of Bath, Bath, U.K., in 1995. He moved to the University of Cambridge, Cambridge, U.K., in 2001, and was elected as a fellow of the Churchill College. He is currently the Chair of the Photonic Integration Research Group, Eindhoven University of Technology. His research interests include integrated photonic circuits. He was a recipient of the Royal Society University Research Fellowship from the University of Bristol, Bristol, U.K., in 1996, the European Commission Marie Curie Chair from the COBRA Institute, also known as the Institute for Photonic Integration, Eindhoven University of Technology, The Netherlands, in 2006, and the Vici Award from The Netherlands Organization for Scientific Research, in 2011, where he has focused on photonic integration technology.